SCIENTIFIC REPORTS

OPEN

SUBJECT AREAS:
HETEROGENEOUS CATALYSIS
CATALYST SYNTHESIS

Received
22 October 2013

Accepted
27 January 2014

Published
10 March 2014

Correspondence and requests for materials should be addressed to Z.Y. (yinzhen@tjpu.edu.cn) or D.M. (dma@pku.edu.cn)

Monodispersed bimetallic PdAg nanoparticles with twinned structures: Formation and enhancement for the methanol oxidation

Zhen Yin[1], Yining Zhang[2], Kai Chen[3], Jing Li[4], Wenjing Li[4], Pei Tang[4], Huabo Zhao[4], Qingjun Zhu[5], Xinhe Bao[6] & Ding Ma[4]

[1]State Key Laboratory of Hollow Fiber Membrane Materials and Processes, Department of Chemical Engineering, Tianjin Polytechnic University, Tianjin 300387, P. R. China, [2]Energy Storage Division, Dalian Institute of Chemical Physics, Chinese Academy of Sciences, Dalian 116023, P. R. China, [3]Chemistry Experimental Teaching Center, University of Science and Technology of China, Hefei 230026, P. R. China, [4]Beijing National Laboratory for Molecular Sciences, College of Chemistry and Molecular Engineering, Peking University, Beijing 100871, China, [5]National Institute of Clean-And-Low-Carbon Energy, Beijing, 102209, China, [6]State Key Laboratory of Catalysis, Dalian Institute of Chemical Physics, Chinese Academy of Sciences, Dalian 116023, P. R. China.

Monodispersed bimetallic PdAg nanoparticles can be fabricated through the emulsion-assisted ethylene glycol (EG) ternary system. Different compositions of bimetallic PdAg nanoparticles, $Pd_{80}Ag_{20}$, $Pd_{65}Ag_{35}$ and $Pd_{46}Ag_{54}$ can be obtained via adjusting the reaction parameters. For the formation process of the bimetallic PdAg nanoparticles, there have two-stage growth processes: firstly, nucleation and growth of the primary nanoclusters; secondly, formation of the secondary nanoparticles with the size-selection and relax process via the coalescence or aggregation of the primary nanoclusters. The as-prepared PdAg can be supported on the carbon black without any post-treatment, which exhibited high electro-oxidation activity towards methanol oxidation under alkaline media. More importantly, carbon-supported $Pd_{80}Ag_{20}$ nanoparticles reveal distinctly superior activities for the methanol oxidation, even if compared with commercial Pt/C electro-catalyst. It is concluded that the enhanced activity is dependant on the unique twinning structure with heterogeneous phase due to the dominating coalescence growth in EG ternary system.

Direct alcohol fuel cells (DAFCs) have attracted remarkable attention as suitable power source for portable electronic devices and electric vehicles[1]. Among a variety of liquid alcohol fuels, methanol has been studied extensively as a promising fuel candidate due to its high energy density, facile handling, low operating cost and various sources such as coal or natural gas. Therefore, considerable efforts have been devoted to the development of electro-catalysts for the direct methanol fuel cells (DMFCs)[2,3]. Although Pt-based catalysts such as PtRu have been recognized as excellent anodic electro-catalysts for DMFCs, many hurdles have to be cleared before they are used in industry due to the high cost and limited supply of Pt[4]. In contrast, it is notable that Pd can be used as the effective catalysts for methanol oxidation, particularly in alkaline media, indicating that Pd is a potential candidate to Pt as the electro-catalyst for alkaline DMFCs in the reality[5,6]. Usually, there are two main methods to enhance electro-catalytic activity of Pd nano-catalysts: one is to fabricate different structure or morphology of Pd electro-catalysts[7–10]; the other is to add second metal element to form bimetallic Pd-based nanoparticles[11–16]. Interestingly, the activity and durability of the bimetallic catalysts can be improved dramatically through modifying the structural and electronic properties of active catalytic sites, e.g., the Pd-Cu and Pd-Au nanoparticles studied in our previous report[17,18]. It is well-known that a number of traditional methods are used for the preparation of bimetallic Pd-based catalysts, such as successive or simultaneous reductions of noble metal precursors with the support. However, the bimetallic nanoparticles obtained from the conventional preparation routine are generally large with relatively wide size distributions, and, more importantly, they rarely display compositional or morphological homogeneity. Hence, the studies to correlate the particle size and composition with catalytic activities are in most cases ambiguous. However, significant successes have been

achieved in the development of Pd-based catalysts despite of their relatively low electro-catalytic activity compared with Pt, there are numerous opportunities for constructing improved Pd-based catalysts[19–22].

To develop reliable and reproducible method for producing large amounts of nano-sized inorganic nanoparticles with uniform size distribution has been a challenge task in materials chemistry research during the last decades. Colloidal methods are particularly useful for fabricating the bimetallic nanoparticles with controlled size and morphology, thereby improving their catalytic activity. However, the formation of monodispersed bimetallic Pd-Ag nanoparticles via colloidal process with designed composition and homogeneous size distribution has been barely successful[23,24]. In our previous report, we synthesized the monodispersed Pd-based bimetallic nanoparticles through emulsion-assisted synthetic strategy on the ternary metal precursor/surfactant/ethylene glycol system, which were applied as effective candidate for the electro-catalysts of DAFCs[25]. The work focused on the ligand-protected bimetallic Pd-based nanoparticles that were served as the building blocks to fabricate the supported bimetallic nanocatalysts because of their size monodispersity, morphology and composition homogeneity. In this present work, monodispersed bimetallic Pd-Ag nanoparticles with different compositions, i.e., $Pd_{80}Ag_{20}$, $Pd_{65}Ag_{35}$ and $Pd_{46}Ag_{54}$ (the numerical subscripts denote the atom ratio of the alloying metal), are firstly fabricated by the modified multiple-phase emulsion-assisted method. This ternary system is therefore proved to be feasible and reproducible method to fabricate bimetallic PdAg nanoparticles and monometallic Ag nanoparticles. More significantly, the prepared bimetallic Pd-Ag or monometallic Pd nanoparticles catalysts, supported over Vulcan XC-72 carbon black powder, are highly active for methanol oxidation even without heat-treatment or any special ligand removal treatment. The catalysts exhibit superior electro-catalytic activity and stability for methanol oxidation in alkaline media compared with the carbon-supported Pd nanoparticles obtained with the same synthesis method, suggesting that are promising candidates in the direct oxidation of methanol. Moreover, carbon-supported $Pd_{80}Ag_{20}$ nanoparticles catalyst prepared in this work exhibited distinctly superior activities for the methanol oxidation, even compared with commercial Pt/C electro-catalyst. We anticipate that this supported colloidal-derived PdAg nanoparticles would lead to improvements in more applications as oxidation catalysts.

Results

The bimetallic PdAg nanoparticles were prepared via the thermal decomposition of palladium acetate and reduction of silver acetate in the emulsion-assisted EG ternary system with the presence of oleylamine (OAm) and oleic acid (OA) as the stabilizing agents[25]. This unique synthetic approach was developed by our group and it is remarkably different from the co-reduction formation process as reported in the literature[23]. The composition of bimetallic PdAg nanoparticles could be adjusted by simply varying the ratio of the concentrations of Pd and Ag precursors and the surfactant amount introduced in the synthesis procedure. The compositions of PdAg nanoparticles, as measured from EDX spectra, were $Pd_{80}Ag_{20}$, $Pd_{65}Ag_{35}$ and $Pd_{46}Ag_{54}$ (Fig. S1, Supporting information), respectively. Fig. 1 shows the TEM images and size distribution of the as-prepared bimetallic PdAg nanoparticles with different compositions.

Obviously, the size of final nanoparticles decreased with an increase of Ag content in the bimetallic nanoparticles. The average size was 3.8 nm (Fig. 1A) for $Pd_{80}Ag_{20}$ nanoparticles, 3.6 nm (Fig. 1B) for $Pd_{65}Ag_{35}$ nanoparticles and 3.3 nm (Fig. 1C) for $Pd_{46}Ag_{54}$ nanoparticles, respectively. Moreover, the size distribution of the nanoparticles narrowed with an increase of Ag content, as shown in Fig. 1. The results indicated that the Ag content could influence the size and size distribution of the bimetallic nanoparticles, which was related to the formation mechanism of bimetallic nanoparticles. However, with further increase of the silver content, the bimetallic nanoparticles can not be fabricated and most of nanoparticles were discrete monometallic Pd or Ag nanoparticles due to the phase segregation in the nucleation process.

Discussion

Formation process of bimetallic nanoparticles from emulsion-assisted EG ternary system. Understanding the mechanism of nanoparticle nucleation and growth is critical for the synthesis of nanoparticles with desired sizes, morphologies, and their physiochemical properties. Nevertheless, it is a challenge task to investigate the microscopic nucleation and growth mechanism because the critical nuclei are extremely unstable and its concentration is very low, especially for the bimetallic nanoparticles[26,27]. Furthermore, most metal nanoparticles prepared via colloidal method are usually synthesized in an aqueous solution or an organic solvent, so the product separation requires the precipitation process meditated by different polar solvents, which could change the size or morphology of the as-prepared particles[28]. However, the peculiarities of the nucleation and growth process in our synthesis can be studied through a series of experimental observation since the product in our emulsion-assisted ternary system can be isolated readily from the reaction mixture via a simple non-polar solvent extraction. The extracted nanoparticles can be dropped directly onto the copper-grid without any post-treatment, thereby reducing the influence of harmful ligands or solvents greatly.

In order to understand the formation mechanism of the PdAg bimetallic nanoparticles, we utilized UV-vis spectroscopy to trace the formation process of PdAg bimetallic nanoparticles. The samples were recovered from the reaction mixture at different temperatures and time intervals. Each sample, after extracted by hexane, was diluted to a fixed volume before the UV-vis measurements were performed. Fig. 2 and Fig. S2 shows UV-vis absorption spectra of the samples dispersed in hexane. The strong absorption at ca. 430 nm was observed when the reaction mixture was heated, which resulted from the excitation of the surface plasmon resonance (SPR) peak of the Ag nanoparticles[30], and indicated that the nucleation of silver clusters occurred at about 90°C according to the solution color change. This adsorption shape remained and shifted to the lower wavelength until 110°C, and turned broad gradually from 120°C. This is believed to be caused by changes in the composition of the products resulted from the thermal decomposition of the palladium acetate at about 115°C[29]. Moreover, no apparent weak feature could be identified in the UV-vis spectrum as the reaction proceeded, confirming that no surface Ag is visible[30]. We propose that Ag nucleates firstly to Ag nanoclusters and grows as the temperature increases. The growing particles are hydrophobically surface-ligated by OA/OAm, and reside within the OA/OAm liquid phase. Subsequently, Pd atoms may deposit or nucleate on the Ag nanoclusters, and the growth might be moderated by the surface ligands, leading to the formation of bimetallic PdAg nanoparticles. Hence, the concentration of silver precursor in the ternary system could influence the particle size and size distribution; resulting in a decrease of the particle size with the increase of the silver precursor concentration (Fig. 1). With high concentration of silver precursor, more silver nanoclusters as seeds are generated and, as a result, the bimetallic PdAg nanoparticles of smaller sizes are formed in the same micro-droplet environment.

Usually, there are two commonly accepted mechanisms for nanoparticle formation: one is the classical LaMer mechanism, which means burst nucleation fast from supersaturated solutions and slow and uniform growth are achieved via diffusion; and the other is Ostwald ripening mechanism, which features dissolving of the smaller nanoparticles to supply nutrient for the growth of the larger nanoparticles due to the chemical potential increase of a particle along with size decrease. Interestingly, another aggregative or

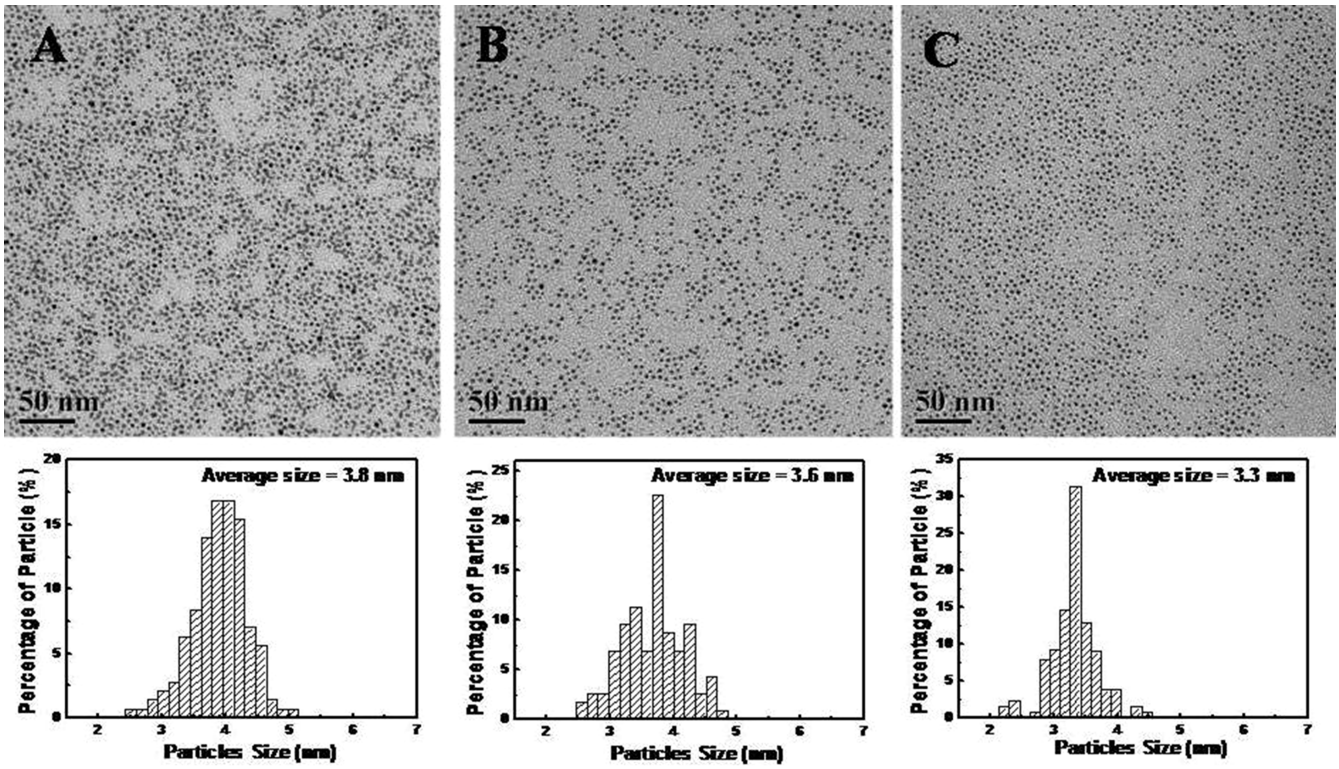

Figure 1 | Representative TEM images and corresponding size distribution of bimetallic PdAg nanoparticles with different compositions at 120°C. (A) $Pd_{80}Ag_{20}$, (B) $Pd_{65}Ag_{35}$ and (C) $Pd_{46}Ag_{54}$.

coalescence mechanism have attracted wide interest in recent years, as confirmed by the direct observation of in-situ TEM[31]. In simple, coalescence growth proceed with the second nucleation process, in which the growth-viable nanoparticles are assembled from primary nanoparticles. To illuminate the formation process of bimetallic PdAg nanoparticles, the TEM and HRTEM were adopted to investigate the products from the reaction system at different reaction stages.

Typical TEM images of the products after 10 min at 120°C are shown in Fig. 3 A–B. The sample mainly contained nearly-spherical particles with bimodal size distribution, smaller particles with size below 5 nm and bigger particles with size above 10 nm (ca. 5%–10%), which exhibited the SPR peak at ca. 430 nm (Fig. 2). As indicated in Fig. 3C–D, the apparent lattice distortion and grain boundaries of particles implicated that most of the particles were comprised of the smaller nanocluster with ca. 1–2 nm size. In addition, these secondary particles contained Ag and Pd elements as evidenced by the EDX analysis. The smaller nanoclusters, as marked by the red arrow in Fig. 3C–D, pointed to the formation of primary particles before the coalescence. Most interestingly, one Pd nanocluster could be identified in Fig. 3F, which was the direct evidence for the nanoparticles coalescence growth via Pd and Ag nanocluster as primary particles. Moreover, some nanoparticles (typically bigger than 10 nm) with multiple-twinned structure, as shown in Fig. 3E, were also observed, revealing the presence of Ag nanoparticles with a lattice spacing of 2.1 Å (200) and 2.4 Å (111), respectively.

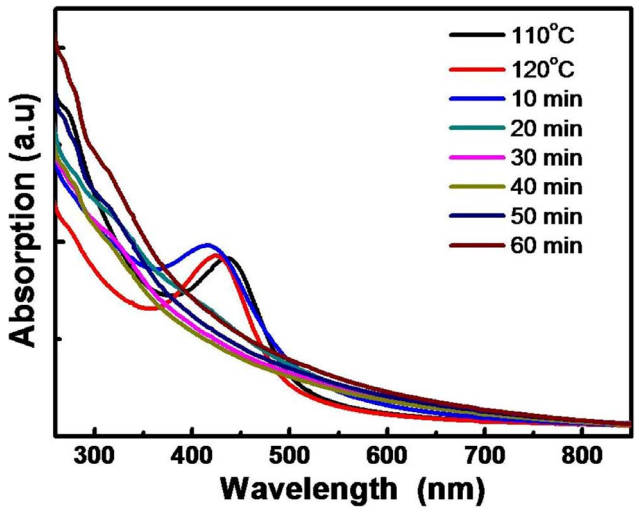

Figure 2 | UV-vis spectra of the typical products at different reaction stages.

When the reaction proceeded for 40 min at 120°C, the big particle (>10 nm) presence was reduced to below 1%, which was also confirmed by the disappearance of SPR peak in the UV-vis spectra (Fig. 2). However, the average size of the secondary particles has no dramatic change with prolonging the reaction time. Some superlattices areas with two layers were visible in Fig. 4A, indicating the occurrence of size selection process. HRTEM images during this stage displayed that the nanoparticles formation were resulted from the coalescence growth in Fig. 4 C–D. However, the small primary nanocluster (ca.1–2 nm) was observed in Fig. 4D, as marked by red arrows, indicating the nucleation process also occurred.

When the reaction time was extended to 60 min, monodispersed spherical nanoparticles with an average diameter of 3.5 nm (standard deviation of 5%), which was a slight decrease compared with the simple combination of the nanocluster size, were obtained (Fig. 5A). The nanoparticles were mostly multiple-twin crystalline (Fig. 5 B–C) with a composition of Pd and Ag, as confirmed by the EDX spectra. In addition, small fraction of the nanoparticles with single crystalline structure was identified. The lattice fringes in the HRTEM image (Fig. 5D) were separated by 2.28 Å that was lower than 2.38 Å of the face-centered cubic (fcc) Ag (111), so it was postulated as the (111) lattice spacing of alloy PdAg nanoparticles with fcc structure.

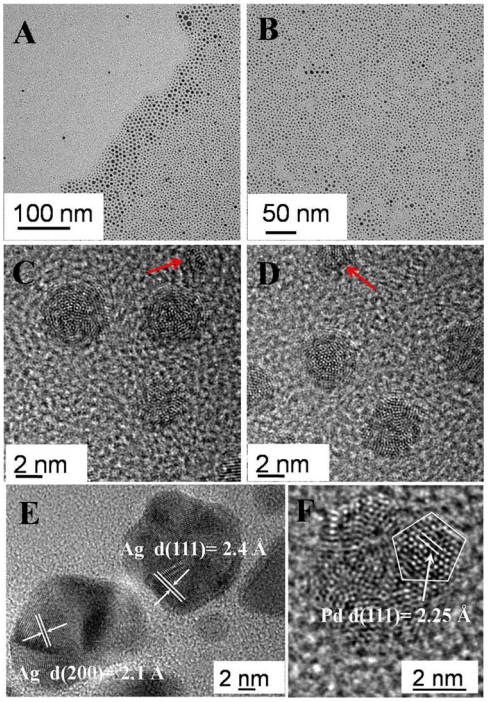

Figure 3 | Representative TEM and HRTEM images of the products at 120°C, 10 min.

During the present stage, there were two simultaneous process: size selection process, which was verified by the complete disappearance of big nanoparticles (>10 nm), and the relax process with a slight decrease of particle size, in which structure and shape could rearrange because of a higher internal energy and chemical potential[31].

It is, therefore, suggested that the formation process of monodispersed bimetallic PdAg nanoparticles have two-stage growth process: firstly, nucleation and growth of the primary nanoclusters; secondly, formation of the secondary nanoparticles with the size-selection and relax process via the coalescence or aggregation of the primary nanoclusters. Most of the primary Pd and Ag nanocluster could aggregate to the secondary particles when the reaction temperature was higher than 115°C, whereas some Ag nanoclusters aggregate to the secondary big Ag particles with the elevating temperatures. And then, these big Ag nanoparticles would dissolve into the solution to supply more monomer in the initial reaction stage indicating from the UV-vis spectra (Fig. 2), and then repeat again the nucleation and coalescence growth process. In this sense, it appears feasible to relate the absorption peak evolution at ca. 400 nm only with the size change of big nanoparticles at initial stage and composition change of the secondary nanoparticles at latter course. Thus, the assumption about the growth mechanism only based on the UV-vis spectra of the whole process, as mentioned above, wasn't fully creditable and completely consistent with the actual experimental results. Based on these facts, it can be concluded that the dominant formation process of the bimetallic PdAg nanoparticles was a nucleation and coalescence growth mechanism, which is illustrated in Fig. 6.

Matijevic et al. developed a new theoretical model of possible formation pathways of monodispersed colloids through the aggregation of nano-size precursors[32–34], and the simple model shed insight on the bimetallic PdAg nanoparticle formation process in our experimental findings. For the aggregation, the size selection can be explained by coupling the dynamical equations for the processes of secondary particle growth by aggregation of subunits and of formation or nucleation of these subunits[32,33]. Indeed, the new formation of the primary nanocluster, as well as the coalescence process of the

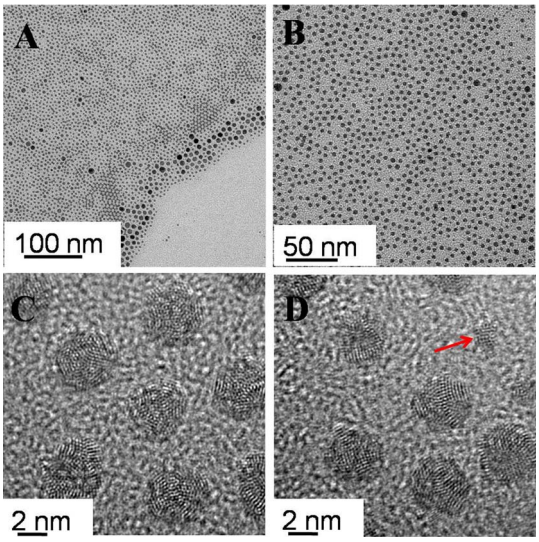

Figure 4 | Representative TEM (A–B) and HRTEM (C–D) images of the products at 120°C, 40 min.

secondary nanoparticles, were observed, as shown in Fig. 5. It was reported that the formation of secondary (final) particles with narrow size distribution was a diffusion-controlled process[35–38], but the diffusion-limited growth can also lead to the narrowing of size distributions in Reiss theoretical research at the micron-sized colloidal systems[39]. In contrast, coalescence growth process model was rarely successful for the application of the nanoparticles synthesis, especially for bimetallic nanoparticles thus far[40]. However, in our ternary system, a great deal of micro-droplets of surfactant with constant size were produced under the condition of vigorous stirring, just like quasi-microemulsion, which could supply the micro-reactor to limit the concentration gradient and diffusion thickness or area of the precursor monomer. Hence, there was a critical size related to monomers concentration in the solution at a fixed concentration which was consistent with colloidal semiconductor growth[41] and resulted in big nanoparticles dissolving and the size selection process. Therefore, the monodispersed bimetallic PdAg nanoparticles with narrow size distribution could only be obtained by constructing micro-reactor with diffusion limitation and concentration constant in this emulsion-assisted ternary system, resulting in the unique dominance of

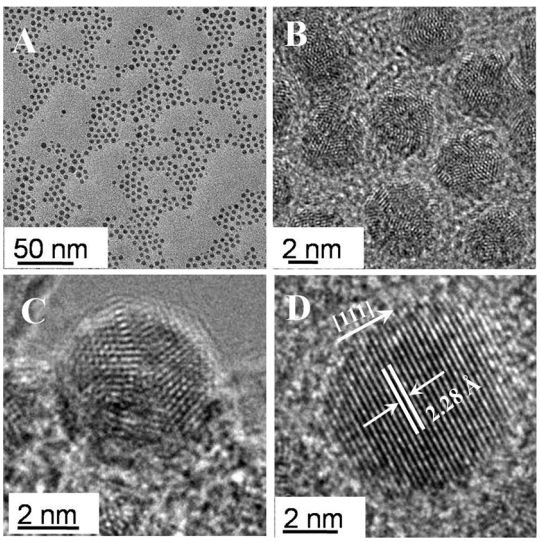

Figure 5 | Representative TEM (A) and HRTEM (B–D) images of bimetallic PdAg nanoparticles at 120°C, 60 min.

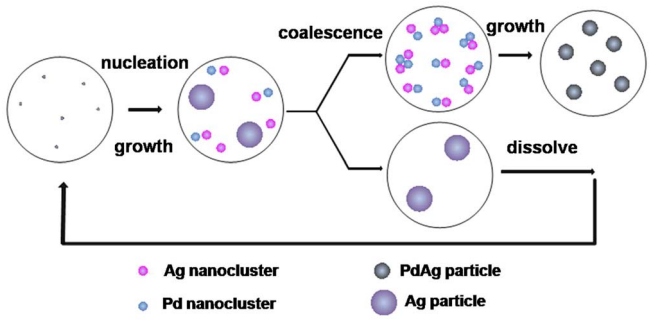

Figure 6 | Schematic representation of the formation process of bimetallic Pd-Ag nanoparticles in the EG ternary system without the Ostwald ripening.

the coalescence growth process. However, the bimetallic PdAg nanoparticles did not form homogeneous phase via such coalescence growth process under the present reaction temperature, which was lower than the homogeneous alloy formation temperature as suggested in the literature[23]. In other words, the bimetallic particles through such formation process could contain the mixture phase, such as alloy phase and Pd segregation, which was verified by the XRD (Fig. 7). As shown in Fig. 7, the diffraction peaks were distinguished at 2θ values of ca. 37° and 43°, respectively, despite of the broad band and low intensity. All patterns displayed fcc phase similar to that of pure Pd nanoparticles. However, shifts to smaller angles were not observed when silver content increased. The results suggest that the bimetallic PdAg particles nanoparticle phase was not homogeneous, and Pd segregation was visible as evidenced by the fact that (111) peak shifted to higher angle. This was the cause for the shoulder peak on the $Pd_{65}Ag_{35}$ nanoparticles. Furthermore, the bimetallic PdAg nanoparticles with abundant multiply or singly twinned structures (Fig. 5) indicate that the peaks could have slightly shifted to the high angle, due to the lattice constant strain in the twinned structures, especially for $Pd_{46}Ag_{54}$[42]. In addition, the particle sizes of PdAg nanoparticles estimated from the XRD patterns were smaller than those measured from the TEM images, confirming the existence of the plentiful twinned structure[42].

In order to confirm the conclusion, the monometallic silver, palladium nanoparticles and the bimetallic PdAg nanoparticles via successive seed growth process were synthesized separately in our EG ternary system. Firstly, only the silver precursor was added into the ternary system and the temperature elevated to 120°C. As shown in Fig. 8 A–B, the Ag nanoparticles with bimodal size distribution could be observed when the temperature was at 115°C. The result substantiated the conclusion from the UV-vis spectra result (Fig. 2 and Fig. S3), and demonstrated the nucleation temperature of the silver was much lower than 115°C. As the reaction proceeded, more silver nanoparticles were formed, leading to big Ag nanoparticles with polyhedral shape and small spherical Ag nanoparticles (Fig. 8 C–D). Although part of the Ag nanoparticles continued to grow, most Ag nanoparticles were formed via the coalescence growth in this stage. When the temperature was kept at 120°C, the size distribution was narrower because of the size selection process in the precursor concentration-constant and diffusion-limitation micro-droplet environment. As shown in Fig. 8E–F, the size distribution of most Ag nanoparticles was very narrow so that the superlattice of Ag nanoparticles can be found on the copper grid. Meanwhile, the proportion of the big Ag nanoparticles was below 1%. When the temperature was cooled to room temperature, the palladium precursor was introduced into the ternary system and the bimetallic Pd-Ag nanoparticles can be observed, as indicated in Fig. 8 G–H and Fig. S3. However, the average size and size distribution were similar to the pristine Ag nanoparticles (Fig. S4), and not much core-shell structures could be identified. Those results illustrated that the bimetallic nanoparticles was formed through the coalescence growth, so most Ag nanoparticles dissolved into the solution, nucleated to form nanocluster and aggregated with the Pd nanoclusters. Our results confirm the versatility of this EG ternary system, even though for the monometallic Ag and Pd nanoparticles, especially size below 5 nm (Fig. S5–S6).

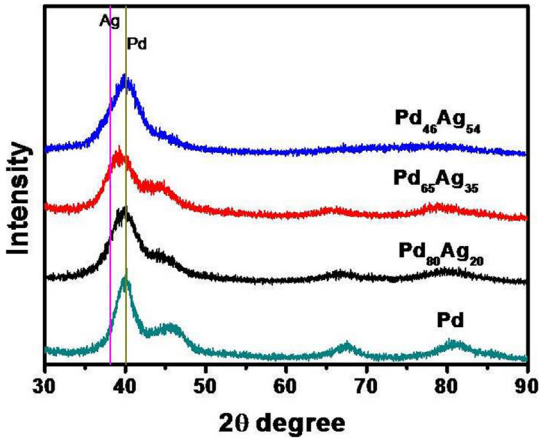

Figure 7 | XRD patterns of PdAg nanoparticles.

Voltammetric characteristics and electrocatalytic activity of supported PdAg nanoparticles on the carbon. The as-prepared bimetallic PdAg nanoparticles can typically deposited onto a solid surface via physical adsorption, such as carbon black without any severe post-treatment. Most of stabilizing ligands can be readily removed by ethanol washing without significantly increasing nanoparticle size or changing nanoparticles morphology, as shown in Fig. 9 and Fig. S7.

TEM images of the catalyst show that most nanoparticles preserved their size and were well-dispersed on the carbon support, as shown in Fig. 9. The particle size and morphology of supported nanoparticles are identical to that of free colloidal PdAg nanoparticles. Moreover, the existence of twinned structures can be observed clearly on the three different PdAg/C catalysts. Hence, our synthesis method show the well-control over PdAg nanoparticle size and size distribution as well as the high nanoparticle dispersity on the support, leading to their favorable use as DAFC catalysts.

The electro-catalytic activities of all catalysts were characterized by cyclic voltammetry (CV) in 1.0 M KOH (Fig. S8) and 1.0 M CH_3OH + 1.0 M KOH solution (Fig. 10), respectively. The CVs of methanol electro-oxidation on the Pd/C, PdAg/C, as well as commercial Pt/C (TKK) catalysts consisted of two parts, i.e., the forward scan and the reverse scan (Fig. 10A). A prominent anodic peak was attributed to the methanol oxidation around −0.1 V in the forward scan. An anodic peak was appreciated in the reverse scan, which was produced by the removal of the incompletely oxidized carbonaceous species formed in the forward scan[43]. These carbonaceous species were mostly in the form of linearly bonded Pd=C=O, and the accumulation of intermediate carbonaceous species on the catalysts surface lead to "catalyst poisoning". Furthermore, an additional cathodic reduction peak at −0.25 V for the $Pd_{65}Ag_{35}$/C and $Pd_{46}Ag_{54}$/C was also observed, which might arise from the reduction of the silver oxide. Obviously, the catalysts of supported bimetallic PdAg nanoparticles on the carbon can promote the oxidation of methanol in alkaline medium remarkably compared with the pure Pd/C catalyst, which was even superior to commercial Pt/C catalyst (TKK).

The catalytic performance of all PdAg/C with different Ag contents, Pd/C and commercial Pt/C catalysts were investigated and compared in the following attributes: the onset potential of methanol oxidation, the anodic peak potential and the forward anodic peak

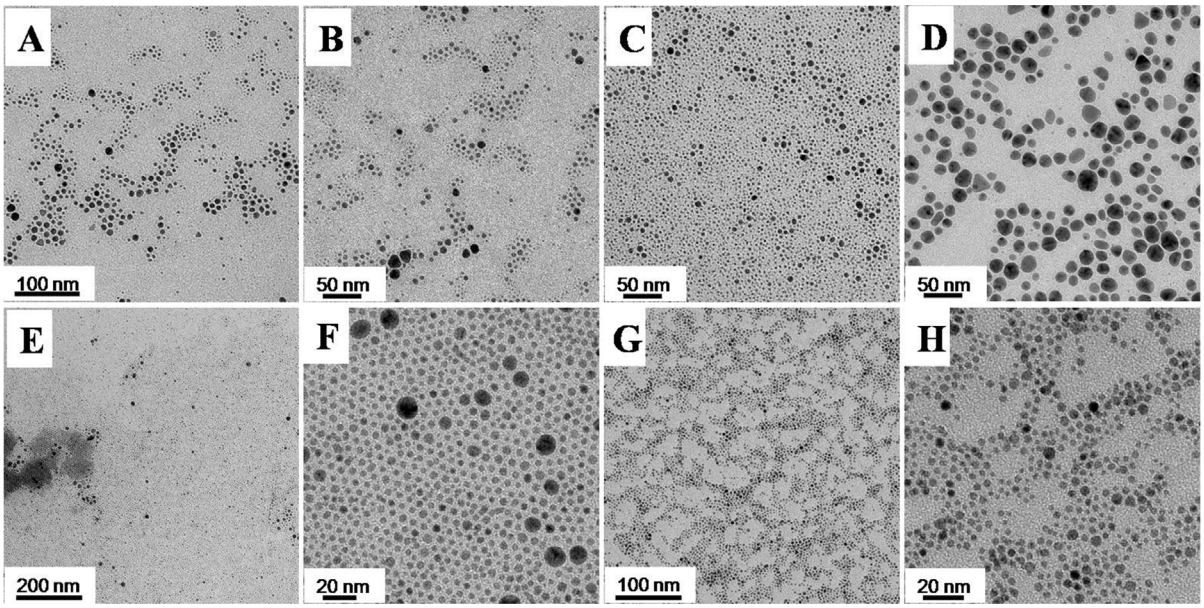

Figure 8 | Representative TEM images of the formation process of the bimetallic PdAg nanoparticles via the successive seed-growth with Ag nanoparticles as the precursors. (A–B) 115°C; (C–D) 120°C; 0 min; (E–F) 120°C, 15 min; (G–H) Pd precursor added, 120°C, 30 min.

current density, and the results are listed in Table 1. It is clear that the incorporation of Ag has shifted the anodic onset potential for the methanol oxidation over the bimetallic Pd-Ag/C catalyst, e.g. about 70 mV towards the negative side in the case of $Pd_{80}Ag_{20}$/C (−0.52 V vs. −0.45 V for Pd/C). These results indicate that the enhancement in the activity for alcohol oxidation on Pd-Ag/C catalyst is not only due to an increase in the surface reaction sites. Moreover, the $Pd_{65}Ag_{35}$/C catalyst shifted the onset potential (~110 mV) towards the negative side, suggesting that available Ag content could improve significantly the kinetics of methanol oxidation. A more important parameter for characterizing the electro-oxidation process is the peak current density achieved. The peak current density was found to increase with the incorporation of Ag into the Pd. The monometallic Pd/C catalyst has a peak current density of 210.5 mA mg^{-1}, which dramatically increased to 691.6 mA mg^{-1} when 20% of the Pd was replaced by Ag, at least three times compared to the pure Pd/C catalyst. More significantly, even compared with that exhibited by the commercial Pt/C (TKK) catalyst, lower anodic peak potential and higher peak current density with $Pd_{80}Ag_{20}$/C indicated that the supported bimetallic $Pd_{80}Ag_{20}$ nanoparticles was superior to the commercial Pt/C catalyst towards methanol electro-oxidation under alkaline media. However, one noticeable point is that the anodic peak in the backward scan was higher than the forward scan for the $Pd_{80}Ag_{20}$/C catalyst, indicating poor direct oxidation of methanol to carbon dioxide during the anodic scan[43,44]. In addition, the bimetallic homogeneous PdAg alloy catalysts can be formed following thermal treatment (in the 5% H_2/argon gas at 400°C for 3 h) without significant morphology or size variety, as indicated in Fig. S9–S10. The diffraction peaks, shifted to small angle and located in between Pd and Ag, turned sharp and intensive, indicating higher degree of crystallinity and homogeneous alloy formation. Although the particle size would have slightly increased, it would display high catalytic

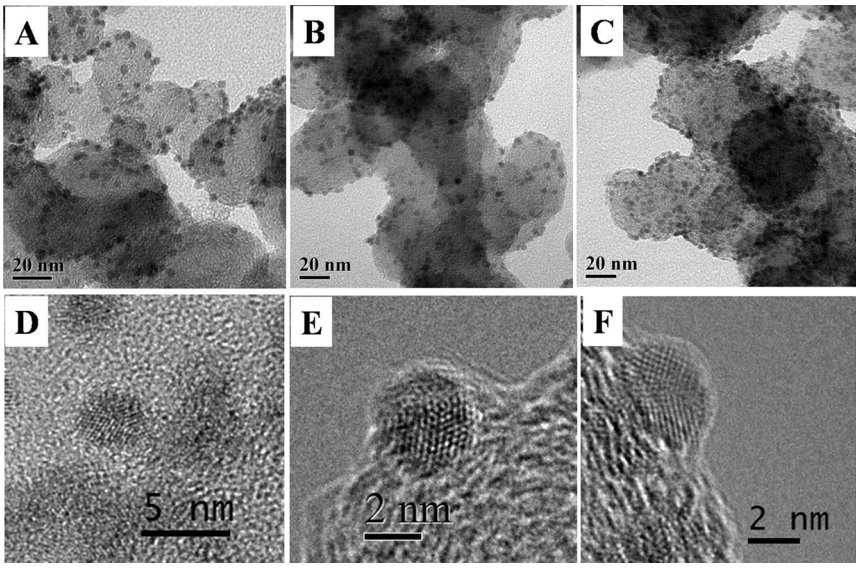

Figure 9 | Representative TEM and HRTEM micrographs of PdAg/C catalysts: $Pd_{80}Ag_{20}$/C (A and D), $Pd_{65}Ag_{35}$/C (B and E) and $Pd_{46}Ag_{54}$/C (C and F). The HRTEM images also revealed the apparent twinned structures. For PdAg nanoparticles, the overall percentage of twinned structures was about 60–80%, which corresponds to XRD results of the unsupported nanoparticles. The HRTEM images were checked by observing at least 50 particles.

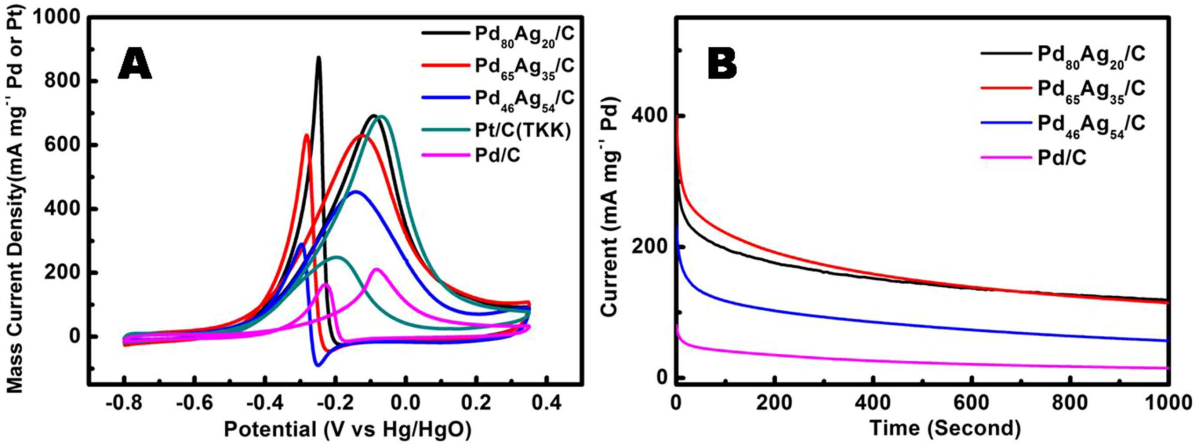

Figure 10 | (A) Cyclic voltammograms of room-temperature methanol oxidation on the Pd/C, PdAg/C and commercial Pt/C (TKK) catalysts in 1 M KOH + 1 M CH_3OH at 50 mV/s. (B) Chronoamperometry measurements of methanol oxidation in 1 M CH_3OH and 1 M KOH solution with PdAg/C catalyst and with Pd/C catalyst at −0.2 V vs. Hg/HgO.

activity towards methanol oxidation after heat-treatment if the homogeneous alloy phase was the vital structure for the bimetallic catalysts. However, the catalytic activity of bimetallic Pd-Ag nanoparticles after heat-treatment was greatly suppressed, though higher than Pd nanoparticles (Fig. S11), implicating that only homogeneous alloy phase may enhance partly the electro-catalytic activity of the PdAg nanoparticles, especially towards methanol oxidation under alkaline media.

The enhanced activity in the present Pd-Ag system with 20% Ag replacement can be attributed following aspects. Firstly, the presence of Ag can accelerate the oxidation of reaction intermediates, especially CO_{ads}[45]. Thus, combination with Ag inhibits the poisoning of the active Pd sites, such as CO_{ads}, this is similar to the Pt-Fe bimetallic system in which the addition of secondary metal Fe facilitates the CO oxidation[46]. On the other hand, the existence of Ag may alter the d-band center of the Pd metal. According to the Hammer and Norskov works via density functional theory (DFT), the d-band center shifts up toward the Fermi level as compared to the parent metals via combination Ag overlayers or Ag impurities with Pd(111) surface, resulting in an increase in the adsorbate binding energy and thus promote the reactivity of Pd for the CO oxidation[47,48]. Secondly, the unique structure of the bimetallic nanoparticle, i.e., heterogeneous phase of the alloy and Pd segregation with plentiful twinned structures. In this structure, twinned boundary would supply considerable defects on the nanoparticles surface and alter the inter-atomic distances due to the lattice strain originated from twin defects, thus may provide more active sites and change the energy levels of bonding electrons for promoting the catalytic properties of the bimetallic nanoparticles[42,49–51]. In addition, the electronic structure modification of the two interactive metallic components could be another important factor for improving catalytic activity[17,18]. As indicated by the XPS spectra of the PdAg/C (Fig. S12), an approximately 0.4–0.5 eV chemical shifts of the Pd 3d core level to higher bind energy were observed in the $Pd_{80}Ag_{20}$/C and $Pd_{65}Ag_{35}$/C catalysts attributed to the strong interaction between Pd and Ag atoms, which could influence the adsorption of methanol or intermediates, resulting in enhancing the electro-activity[24].

The long-term stabilities of PdAg/C catalysts, Pd/C catalyst towards methanol oxidation were investigated with chronoamperometric curves in 1 M methanol + 1 M KOH. As shown in Fig. 10B, the current decayed rapidly with the Pd/C and bimetallic PdAg/C catalysts within 100 s and then slowly to approach the limiting currents for more than 1000 s, but the mass current density with the bimetallic PdAg/C catalysts were at least four times higher than that with the pure Pd/C catalyst even though the oxidation reaction reached the steady state, especially about eight times with $Pd_{80}Ag_{20}$/C catalyst. Meanwhile, the long-term stability of PdAg/C catalyst was still not as good as commercial Pt/C catalysts. Chronoamperometric characterization further confirmed that supported bimetallic PdAg nanoparticles had better steady state electrolysis activity than pure supported Pd nanoparticles for methanol oxidation in an alkaline media, which again suggesting that bimetallic PdAg/C catalyst with 20% Ag replacement has considerable potential to be used as non-Pt electro-catalyst for DAFCs.

In conclusion, monodisperse bimetallic PdAg nanoparticles with controllable size and compositions have been synthesized via emulsion-assisted EG ternary system. The formation process was discussed in details via the UV-vis, TEM and HRTEM approach. The dominant formation process of the bimetallic PdAg nanoparticles was a nucleation and coalescence growth mechanism under quasi-microemulsion micro-reactor, farther construction of the heterogeneous phase containing alloy and Pd segregation along with vast twinned structures.

The electrochemical tests exhibited that the bimetallic PdAg/C catalysts had remarkably higher catalytic activity toward methanol oxidation reaction compared to the pure Pd/C catalyst. Particular $Pd_{80}Ag_{20}$/C catalyst has lower onset potential, higher peak current density and superior electro-catalytic activity, even better than commercially available Pt/C catalysts. The high activity of the supported bimetallic $Pd_{80}Ag_{20}$ nanoparticles is obviously due to the unique

Table 1 | Electrochemical Properties and Performance of the Different Catalysts

Catalysts	Onset Potential (V vs. Hg/HgO)	Anodic Peak Potential (V vs. Hg/HgO)	Anodic Peak Current (mA mg^{-1} Pd or Pt)
Pd/C	−0.45	−0.08	210.5
$Pd_{80}Ag_{20}$/C	−0.52	−0.091	691.6
$Pd_{65}Ag_{35}$/C	−0.56	−0.13	629.6
$Pd_{46}Ag_{54}$/C	−0.52	−0.14	453.4
Pt/C(TKK)	−0.52	−0.07	689.3

mixed structures with twin defects, electronic effect resulting from alloying with silver. Furthermore, nano-size, monodispersity of the catalyst particles and excellent dispersion of the catalysts on the carbon support by colloidal deposition would have positive impact on tuning the catalytic activity. Thus, colloidal synthesis of bimetallic PdAg nanoparticles via the EG ternary system displays significant potential as less expensive electro-catalyst for alcohol electro-oxidation in alkaline media in DAFCs. More generally, for bimetallic nanoparticles, this work provides a better understanding of formation mechanisms involved in coalescence growth resulting in twin structure and thus tailoring their catalytic properties.

Mechanistic studies on electrochemical properties of the PdAg catalysts and application of PdAg nanoparticles on other heterogeneous catalytic reaction are in progress.

Methods

Chemicals. Oleic acid (OA, Alfa Aesar, 90%, tech) and oleylamine (OAm, Acros, 97%) were used as received. Palladium acetate and silver acetate were purchased from Sino-Platinum Metals Co., Ltd and Tianjin Fuchen Chemical Reagent Co., Ltd, respectively. EG was purchased from Sinopharm Chemical Reagent Co., Ltd. All chemicals used in our experiments were purchased and used as received without further purification. Aqueous solutions were prepared with the water purified through a Millipore system (18.2 MΩ·cm). Commercially available catalyst of 28.4 wt% Pt/C was obtained from TKK.

Synthesis of bimetallic PdAg nanoparticles. The synthesis and characterization of the bimetallic PdAg nanoparticles stabilized by oleylamine and oleic acid have been described in our previous paper. All synthesis was carried out under argon atmosphere. In a typical procedure for the synthesis of $Pd_{46}Ag_{54}$ (the numerical subscripts denote the atom ratio of the alloying metal) nanoparticles as an example, 1.5 mmol oleic acid (OA) and 1.5 mmol oleylamine (OAm) were mixed with 50 mL EG in a three-necked round-bottom flask equipped with mechanical stirring and a reflux condenser to form turbid solution under vigorous stir. And then, two metal precursor solution of 0.5 mmol $Pd(CH_3COO)_2$ in acetone and 0.5 mmol $Ag(CH_3COO)$ in water were added. The mixture was stirred vigorously and heated to 120°C and kept at this temperature for 60–90 min with argon flow passing through the reaction system to take away water and acetone and other organic byproducts. The as-prepared colloidal nanoparticles dispersions were separated through extraction with hexane from the mixture when it was cooled down to room temperature. The colloidal solution was concentrated in a rotary evaporator and then excessive ethanol was added to the slimy solution to yield a black solid, which was separated by centrifugation (10000 rpm for 15–20 min), washed with the mixture of hexane and ethanol for several times until the supernatant solution was clear. The black nanoparticles precipitate can be easily re-dispersed in non-polar organic solvent, such as hexane or toluene.

$Pd_{80}Ag_{20}$ and $Pd_{65}Ag_{35}$ of the bimetallic PdAg nanoparticles were also prepared by the same procedure with 5 : 1 molar ratio of palladium acetate to silver acetate and 1 : 1 molar ratio of OAm to OA were added in synthesis, except different adding amount of surfactants. For $Pd_{80}Ag_{20}$ and $Pd_{65}Ag_{35}$ nanoparticles synthesis, the amounts of OAm and OA were 1.5 mmol and 3 mmol, respectively.

Synthesis of monodisperse Pd nanoparticles. Pd nanoparticles were synthesized under similar reaction condition but with keeping temperature at 120°C for 30–60 min.

Loading PdAg nanoparticles on a carbon support (PdAg/C). Typically, the colloidal suspension of PdAg was taken up in hexane (100 mL), and then the Vulcan XC-72 carbon black (Cabot) powder was added. The slurry was stirred in air at room temperature for about 15 min following the ultrasonic treatment for ca. 3–4 hours. The solid phase was separated by centrifuge after several washing times with excessive ethanol, and dried in an oven under vacuum at 55°C for another 6 hours to obtain the supported catalyst. The loading of carbon-supported PdAg catalysts (PdAg/C) corresponds to the colloidal suspension concentration of PdAg nanoparticles based on an inductively coupled plasma-atomic emission spectrometry (ICP) results. Moreover, with this method it is easy to vary the nanoparticles loading without the varying size distribution or the morphology of nanoparticles.

The carbon-supported as-prepared Pd nanoparticles catalyst (Pd/C) was prepared in a similar way.

Characterization. Transmission electron microscopy (TEM) specimens were prepared by dispersing the suspension of nanoparticles in hexane and drop-casting it onto TEM copper-grids. TEM images were recorded on a FEI Tecnai G2 Spirit microscope equipped with a Gatan CCD camera and with an energy dispersive X-ray (EDX) system from EDAX Inc. at an accelerating voltage of 120 kV. The high resolution TEM (HR-TEM) images were recorded on a FEI Tecnai G2 microscope at an accelerating voltage of 300 kV equipped with an energy dispersive X-ray (EDX) system from EDAX Inc. with a point resolution of 0.20 nm. Powder X-ray diffraction (PXRD) patterns were taken using a Rigaku D/max-2500 diffractometer with a Cu Kα X-ray source (λ = 1.5405 Å) operated at 40 kV with a scan rate of 0.083° 2θ/s. The composition of nanoparticles was analyzed by an inductively coupled plasma-atomic emission spectrometry (LEEMAN, PLASMA-SPEC-II). The particle size distribution was obtained by analyzing at least 200 particles on the TEM images using the Image software from Gatan in this work. The UV-vis spectra were acquired with a JASCO V-550 spectrophotometer from 300 to 900 nm. Nanoparticles solutions were in hexane.

Electrochemical measurement. The electrocatalysis measurement was performed with a CHI 600B electrochemistry workstation with a RDE system (EG&G model 636). A standard three-electrode electrochemical cell was used. The working electrode was a thin layer of Nafion-impregnated catalyst cast on a glassy carbon electrode (GCE) (4 mm in diameter) prepared as follows: the catalyst slurry was first prepared by mixing 1 mL of isopropanol, 5 mg of catalyst and 50 μL of Nafion (5 wt%, DuPont) ultrasonically for 30 min to get the catalyst ink. Then 10 μL of this ink was transferred onto a freshly polished GCE embedded in a Teflon mold by a syringe, followed by natural evaporation of solvent in air. A Pt wire was used as the counter electrode, and an Hg/HgO/1 M KOH electrode (0.098 V vs. SHE) served as the reference electrode. Before CV measurements were recorded, the electrolyte was purged with nitrogen for 30 min, and several tens of CV cycles (sweeping rate: 50 $mV \cdot s^{-1}$) were performed between −0.8 and 0.35 V to stabilize the electrode surface. Cyclic voltammograms (CVs) were carried out at room temperature in 1.0 M methanol + 1.0 M KOH solution, which was degassed with N_2 prior to the experiments and N_2 bubbling was maintained during the measurements. All potentials were referred to the Hg/HgO/1 M KOH electrode in this paper.

1. Antolini, E. & Gonzalez, E. R. Alkaline direct alcohol fuel cells. *J. Power Sources* **195**, 3431–3450 (2010).
2. Wang, C.-Y. Fundamental Models for Fuel Cell Engineering. *Chem. Rev.* **104**, 4727–4766 (2004).
3. Liu, H. S. *et al.* A review of anode catalysis in the direct methanol fuel cell. *J. Power Sources* **155**, 95–110 (2006).
4. Serov, A. & Kwak, C. Review of non-platinum anode catalysts for DMFC and PEMFC application. *Appl. Catal. B-Environ.* **90**, 313–320 (2009).
5. Antolini, E. Palladium in fuel cell catalysis. *Energy Environ. Sci.* **2**, 915–931 (2009).
6. Bianchini, C. & Shen, P. K. Palladium-Based Electrocatalysts for Alcohol Oxidation in Half Cells and in Direct Alcohol Fuel Cells. *Chem. Rev.* **109**, 4183–4206 (2009).
7. Yin, Z., Zheng, H. J., Ma, D. & Bao, X. H. Porous Palladium Nanoflowers that Have Enhanced Methanol Electro-Oxidation Activity. *J. Phys. Chem. C* **113**, 1001–1005 (2009).
8. Ge, J. *et al.* Controllable Synthesis of Pd Nanocatalysts for Direct Formic Acid Fuel Cell (DFAFC) Application: From Pd Hollow Nanospheres to Pd Nanoparticles. *J. Phys. Chem. C* **111**, 17305–17310 (2007).
9. Huang, X., Tang, S., Zhang, H., Zhou, Z. & Zheng, N. Controlled Formation of Concave Tetrahedral/Trigonal Bipyramidal Palladium Nanocrystals. *J. Am. Chem. Soc.* **131**, 13916–13917 (2009).
10. Shen, Q. *et al.* Morphology-Controlled Synthesis of Palladium Nanostructures by Sonoelectrochemical Method and Their Application in Direct Alcohol Oxidation. *J. Phys. Chem. C* **113**, 1267–1273 (2009).
11. He, Q. G., Chen, W., Mukerjee, S., Chen, S. W. & Laufek, F. Carbon-supported PdM (M = Au and Sn) nanocatalysts for the electrooxidation of ethanol in high pH media. *J. Power Sources* **187**, 298–304 (2009).
12. Bunazawa, H. & Yamazaki, Y. Ultrasonic synthesis and evaluation of non-platinum catalysts for alkaline direct methanol fuel cells. *J. Power Sources* **190**, 210–215 (2009).
13. Xu, C. W., Tian, Z. Q., Chen, Z. C. & Jiang, S. P. Pd/C promoted by Au for 2-propanol electrooxidation in alkaline media. *Electrochem. Commun.* **10**, 246–249 (2008).
14. Liu, Z. L., Zhang, X. H. & Hong, L. Physical and electrochemical characterizations of nanostructured Pd/C and PdNi/C catalysts for methanol oxidation. *Electrochem. Commun.* **11**, 925–928 (2009).
15. Nguyen, S. T. *et al.* Enhancement effect of Ag for Pd/C towards the ethanol electro-oxidation in alkaline media. *Appl. Catal. B-Environ.* **91**, 507–515 (2009).
16. Jou, L.-H., Chang, J.-K., Whang, T.-J. & Sun, I. W. Electrodeposition of Palladium--Tin Alloys from 1-Ethyl-3-methylimidazolium Chloride-Tetrafluoroborate Ionic Liquid for Ethanol Electro-Oxidation. *J. Electrochem. Soc.* **157**, D443–D449 (2010).
17. Yin, Z. *et al.* Supported Pd-Cu Bimetallic Nanoparticles That Have High Activity for the Electrochemical Oxidation of Methanol. *Chem. Eur. J.* **18**, 4887–4893 (2012).
18. Yin, Z. *et al.* Supported bimetallic PdAu nanoparticles with superior electrocatalytic activity towards methanol oxidation. *J. Mater. Chem. A* **1**, 9157–9163 (2013).
19. Sankar, M. *et al.* Designing bimetallic catalysts for a green and sustainable future. *Chem. Soc. Rev.* **41**, 8099–8139 (2012).
20. Ferrando, R., Jellinek, J. & Johnston, R. L. Nanoalloys: From Theory to Applications of Alloy Clusters and Nanoparticles. *Chem. Rev.* **108**, 845–910 (2008).
21. Hutchings, G. J. Nanocrystalline gold and gold-palladium alloy oxidation catalysts: a personal reflection on the nature of the active sites. *Dalton Trans.* 5523–5536 (2008).

22. Kariuki, N. N. *et al.* Colloidal Synthesis and Characterization of Carbon-Supported Pd-Cu Nanoparticle Oxygen Reduction Electrocatalysts. *Chem. Mater.* **22**, 4144–4152 (2010).
23. Zhang, S., Metin, O., Su, D. & Sun, S. Monodisperse AgPd Alloy Nanoparticles and Their Superior Catalysis for the Dehydrogenation of Formic Acid. *Angew. Chem., Int. Ed.* **52**, 3681–3684 (2013).
24. Slanac, D. A., Hardin, W. G., Johnston, K. P. & Stevenson, K. J. Atomic Ensemble and Electronic Effects in Ag-Rich AgPd Nanoalloy Catalysts for Oxygen Reduction in Alkaline Media. *J. Am. Chem. Soc.* **134**, 9812–9819 (2012).
25. Yin, Z., Ma, D. & Bao, X. H. Emulsion-assisted synthesis of monodisperse binary metal nanoparticles. *Chem. Commun.* **46**, 1344–1346 (2010).
26. Auer, S. & Frenkel, D. Prediction of absolute crystal-nucleation rate in hard-sphere colloids. *Nature* **409**, 1020–1023 (2001).
27. Shevchenko, E. V. *et al.* Study of Nucleation and Growth in the Organometallic Synthesis of Magnetic Alloy Nanocrystals: The Role of Nucleation Rate in Size Control of CoPt3 Nanocrystals. *J. Am. Chem. Soc.* **125**, 9090–9101 (2003).
28. Lim, B., Yu, T., Park, J., Zheng, Y. Q. & Xia, Y. N. Mixing an Aqueous Suspension of Pd or Au Nanocrystals with a Less Polar Solvent Can Cause Changes to Size, Morphology, or Both. *Angew. Chem., Int. Ed.* **50**, 6052–6055 (2011).
29. Tano, T., Esumi, K. & Meguro, K. Preparation of organopalladium sols by thermal decomposition of palladium acetate. *J. Colloid Interface Sci.* **133**, 530–533 (1989).
30. Lin, X. Z., Teng, X. & Yang, H. Direct Synthesis of Narrowly Dispersed Silver Nanoparticles Using a Single-Source Precursor. *Langmuir* **19**, 10081–10085 (2003).
31. Zheng, H. M. *et al.* Observation of Single Colloidal Platinum Nanocrystal Growth Trajectories. *Science* **324**, 1309–1312 (2009).
32. Park, J., Privman, V. & Matijevic, E. Model of formation of monodispersed colloids. *J. Phys. Chem. B* **105**, 11630–11635 (2001).
33. Goia, D. V. & Matijevic, E. Tailoring the particle size of monodispersed colloidal gold. *Colloids Surf., A* **146**, 139–152 (1999).
34. Privman, V., Goia, D. V., Park, J. & Matijevic, E. Mechanism of formation of monodispersed colloids by aggregation of nanosize precursors. *J. Colloid Interface Sci.* **213**, 36–45 (1999).
35. Matijevic, E. Production of monodispersed colloidal particles. *Annu. Rev. Mater. Sci.* **15**, 483–516 (1985).
36. Sugimoto, T. Preparation of monodispersed colloidal particles. *Adv. Colloid Interface Sci.* **28**, 65–108 (1987).
37. Matijevic, E. Preparation and properties of uniform size colloids. *Chem. Mater.* **5**, 412–426 (1993).
38. Matijevic, E. Uniform inorganic colloid dispersions - achievements and challenges. *Langmuir* **10**, 8–16 (1994).
39. Reiss, H. The growth of uniform colloidal dispersions. *J. Chem. Phys.* **19**, 482–487 (1951).
40. Lim, B. *et al.* Twin-Induced Growth of Palladium-Platinum Alloy Nanocrystals. *Angew. Chem., Int. Ed.* **48**, 6304–6308 (2009).
41. Peng, X., Wickham, J. & Alivisatos, A. P. Kinetics of II–VI and III–V Colloidal Semiconductor Nanocrystal Growth: "Focusing" of Size Distributions. *J. Am. Chem. Soc.* **120**, 5343–5344 (1998).
42. Lee, Y., Loew, A. & Sun, S. Surface- and Structure-Dependent Catalytic Activity of Au Nanoparticles for Oxygen Reduction Reaction. *Chem. Mater.* **22**, 755–761 (2010).
43. Manohara, R. & Goodenough, J. B. Methanol oxidation in acid on ordered NiTi. *J. Mater. Chem.* **2**, 875 (1992).
44. Huang, J., Liu, Z., He, C. & Gan, L. M. Synthesis of PtRu Nanoparticles from the Hydrosilylation Reaction and Application as Catalyst for Direct Methanol Fuel Cell. *J. Phys. Chem. B* **109**, 16644–16649 (2005).
45. Wang, Y., Sheng, Z. M., Yang, H. B., Jiang, S. P. & Li, C. M. Electrocatalysis of carbon black- or activated carbon nanotubes-supported Pd-Ag towards methanol oxidation in alkaline media. *Int. J. Hydrog. Energy* **35**, 10087–10093 (2010).
46. Fu, Q. *et al.* Interface-Confined Ferrous Centers for Catalytic Oxidation. *Science* **328**, 1141–1144 (2010).
47. Ruban, A., Hammer, B., Stoltze, P., Skriver, H. L. & Norskov, J. K. Surface electronic structure and reactivity of transition and noble metals. *J. Mol. Catal. A* **115**, 421–429 (1997).
48. Hammer, B. & Norskov, J. K. Theoretical surface science and catalysis - Calculations and concepts. *Adv. Catal.* **45**, 71 (2000).
49. Marks, L. D. & Howie, A. Multiply-twinned particles in silver catalysts. *Nature* **282**, 196–198 (1979).
50. Bao, J. M. *et al.* Optical properties of rotationally twinned InP nanowire heterostructures. *Nano Lett.* **8**, 836–841 (2008).
51. Smith, A. M., Mohs, A. M. & Nie, S. Tuning the optical and electronic properties of colloidal nanocrystals by lattice strain. *Nature Nanotechnol.* **4**, 56–63 (2009).

Acknowledgments

This work was supported by the National Natural Science Foundation of China (21173009, 21222306, 21303119), 973 Project (2013CB933100), and High School Science & Technology Fund Planning Project of Tianjin (20120513). We gratefully acknowledge the contributions of Professor Wuzong Zhou for discussion about the particles formation mechanism from University of St. Andrews; Professor Jian Chen for assistance and discussion on the electrochemical measurements, Dr. Rentao Mu for discussion on the XPS spectra, from Dalian Institute of Chemical Physics, Chinese Academy of Science.

Author contributions

Z.Y. and D.M. conceived and performed the experiments, analyzed results, and wrote the paper. Y.Z. and K.C. involved in collecting and analysing the data. J.L., W.L., P.T., H.Z. and Q.Z. helped to characterize the samples and analyse the results. Q.Z. and X.B. involved in analysing the results and writing the paper.

Additional information

Supplementary information accompanies this paper at http://www.nature.com/scientificreports

Competing financial interests: The authors declare no competing financial interests.

How to cite this article: Yin, Z. *et al.* Monodispersed bimetallic PdAg nanoparticles with twinned structures: Formation and enhancement for the methanol oxidation. *Sci. Rep.* **4**, 4288; DOI:10.1038/srep04288 (2014).